Inorganic Chemistry

Article

Synthetic Models of the Reduced Active Site of Superoxide Reductase

Jason A. Halfen,* Heather L. Moore, and Derek C. Fox

Department of Chemistry, University of Wisconsin-Eau Claire, 105 Garfield Avenue, Eau Claire, Wisconsin 54702

We report the synthesis, structural and spectroscopic characterization, and magnetic and electrochemical studies of a series of iron(II) complexes of the pyridyl-appended diazacyclooctane ligand L^8py_2, including several that model the square-pyramidal [$Fe^{II}(N_{his})_4(S_{cys})$] structure of the reduced active site of the non-heme iron enzyme superoxide reductase. Combination of L^8py_2 with $FeCl_2$ provides [$L^8py_2FeCl_2$] (**1**), which contains a trigonal-prismatic hexacoordinate iron(II) center, whereas a parallel reaction using [$Fe(H_2O)_6$](BF_4)$_2$ provides [$L^8py_2Fe(FBF_3)$]BF_4 (**2**), a novel BF_4^--ligated square-pyramidal iron(II) complex. Substitution of the BF_4^- ligand in **2** with formate or acetate ions affords distorted pentacoordinate [$L^8py_2Fe(O_2CH)$]BF_4 (**3**) and [$L^8py_2Fe(O_2CCH_3)$]BF_4 (**4**), respectively. Models of the superoxide reductase active site are prepared upon reaction of **2** with sodium salts of aromatic and aliphatic thiolates. These model complexes include [$L^8py_2Fe(SC_6H_4-p-CH_3)$]$BF_4$ (**5**), [$L^8py_2Fe(SC_6H_4-m-CH_3)$]$BF_4$ (**6**), and [$L^8py_2Fe(SC_6H_{11})$]BF_4 (**7**). X-ray crystallographic studies confirm that the iron(II)–thiolate complexes model the square-pyramidal geometry and N_4S donor set of the reduced active site of superoxide reductase. The iron(II)–thiolate complexes are high spin ($S = 2$), and their solutions are yellow in color because of multiple charge-transfer transitions that occur between 300 and 425 nm. The ambient temperature cyclic voltammograms of the iron(II)–thiolate complexes contain irreversible oxidation waves with anodic peak potentials that correlate with the relative electron donating abilities of the thiolate ligands. This electrochemical irreversibility is attributed to the bimolecular generation of disulfides from the electrochemically generated iron(III)–thiolate species.

Introduction

Nature has devised several pathways for the detoxification of superoxide (O_2^-) in biological systems.[1] The most familiar routes involve superoxide dismutases, a diverse group of metalloenzymes that mediate the conversion of superoxide to both hydrogen peroxide and dioxygen.[2] An alternative pathway to superoxide dismutation is the one-electron reduction of superoxide, a process mediated by the recently characterized group of metalloenzymes known as superoxide reductases (SORs).[3] These non-heme iron enzymes are produced by anaerobes and microaerophiles that cannot

tolerate the dioxygen coproduct formed during superoxide dismutation. Structural studies of the reduced SOR (SOR$_{Red}$) active site reveal an iron(II) ion bound by a square-pyramidal array of four equatorial histidine imidazoles and a single, axial cysteine thiolate ligand (Figure 1).[4] Superoxide is proposed to bind to the metal center *trans* to the cysteinate ligand; single electron transfer from the iron and subsequent protonation of the bound peroxide generates hydrogen peroxide and the iron(III) form of the enzyme.[5] As part of our examination of metal-mediated superoxide detoxification pathways in biology, we have targeted synthetic models of SOR$_{Red}$ for preparation, characterization, and reactivity studies.

(1) (a) Fridovich, I. *J. Exp. Biol.* **1998**, *201*, 1203−1209. (b) Fridovich, I. *J. Biol. Chem.* **1997**, *272*, 18515−81517. (b) Fridovich, I. *Annu. Rev. Biochem.* **1995**, *64*, 97−112.
(2) (a) Lyons, T. J.; Gralla, E. B.; Valentine, J. S. *Met. Ions Biol. Sys.* **1999**, *36*, 125−177. (b) Lah, M. S.; Dixon, M. M.; Pattridge, K. A.; Stallings, W. C.; Fee, J. A.; Ludwig, M. L. *Biochemistry* **1995**, *34*, 1646−1660. (c) Hsu, J.-L.; Hsieh, Y.; Tu, C. K.; O'Connor, D.; Nick, H. S.; Silverman, D. N. *J. Biol. Chem.* **1996**, *271*, 17687−17691. (d) Youn, H.-D.; Kim, E.-J.; Roe, J.-H.; Hah, Y. C.; Kang, S.-O. *Biochem. J.* **1996**, *318*, 889−896.

(3) (a) Jenney, F. E., Jr.; Verhagen, M. F. J. M.; Cui, X.; Adams, M. W. W. *Science* **1999**, *286*, 306−309. (b) Jovanovic, T.; Ascenso, C.; Hazlett, K. R. O.; Sikkink, R.; Krebs, C.; Litwiller, R.; Benson, L. M.; Moura, I.; Moura, J. J. G.; Radolf, J. D.; Huynh, B. H.; Naylor, S.; Rusnak, F. *J. Biol. Chem.* **2000**, *275*, 28439−28448.
(4) (a) Coelho, A. V.; Matias, P.; Fulop, V.; Thompson, A.; Gonzalez, A.; Coronado, M. A. *J. Biol. Inorg. Chem.* **1997**, *2*, 680−689. (b) Yeh, A. P.; Hu, Y.; Jenner, F. E., Jr.; Adams, M. W. W.; Rees, D. C. *Biochemistry* **2000**, *39*, 2499−2508. (c) Clay, M. D.; Jenney, F. E., Jr.; Hagedoorn, P. L.; George, G. N.; Adams, M. W. W.; Johnson, M. K. *J. Am. Chem. Soc.* **2002**, *124*, 788−805.
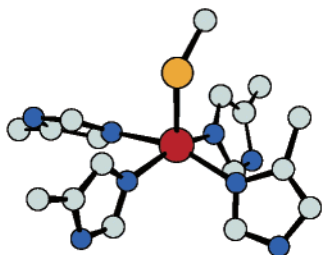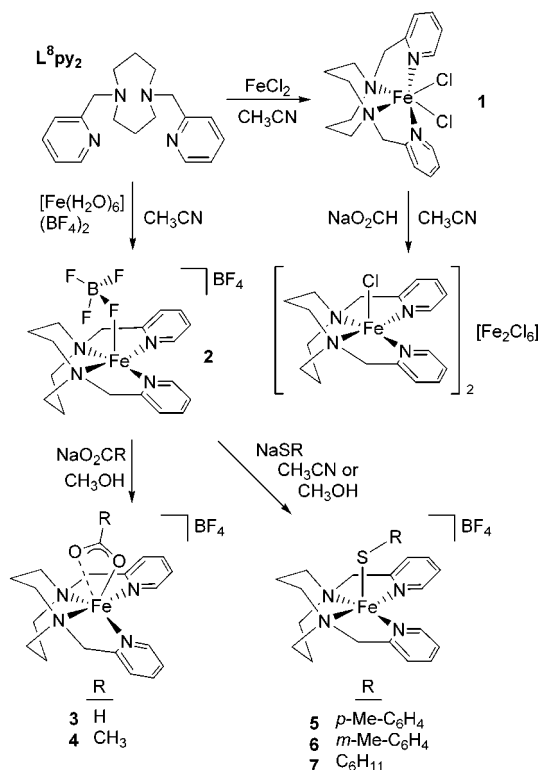
Figure 1. Reduced active site of superoxide reductase as determined by X-ray crystallography (ref 4b).

Scheme 1

We recently described the synthesis of a pyridyl-appended diazacyclooctane ligand, L^8py_2 (Scheme 1), and its use in the preparation of Cu(II) catalysts for olefin aziridination.[6] Examination of Ni(II) and Co(II) complexes of L^8py_2 has revealed that the tetradentate ligand most often occupies the four equatorial coordination sites of square-planar or square-pyramidal transition metal complexes.[7] Herein, we describe the coordination chemistry of L^8py_2 with Fe(II) and report

(5) (a) Coulter, E. D.; Emerson, J. P.; Kurtz, D. A., Jr.; Cabelli, D. E. *J. Am. Chem. Soc*. **2000**, *122*, 11555−11556. (b) Lombard, M.; Fontecave, M.; Touati, D.; Nivière, V. *J. Biol. Chem*. **2000**, *275*, 115−121. (c) Lombard, M.; Houee-Levin, C.; Touati, D.; Fontecave, M.; Nivière, V. *Biochemistry* **2001**, *40*, 5032−5040. (d) Nivière, V.; Lombard, M.; Fontecave, M.; Houee-Levin, C. *FEBS Lett*. **2001**, *497*, 171−173. (e) Emerson, J. P.; Coulter, E. D.; Cabelli, D. E.; Phillips, R. S.; Kurtz, D. M., Jr. *Biochemistry* **2002**, *41*, 4348−4357. (f) Mathé, C.; Mattioli, T. A.; Horner, O.; Lombard, M.; Latour, J.-M.; Fontecave, M.; Nivière, V. *J. Am. Chem. Soc*. **2002**, *124*, 4966−4967.
(6) L^8py_2 = 1,5-bis(2-pyridylmethyl)-1,5-diazacyclooctane: Halfen, J. A.; Fox, D. C.; Mehn, M. P.; Que, L., Jr. *Inorg. Chem*. **2000**, *39*, 4913−4920.
(7) (a) Du, M.; Shang, Z.-L.; Leng, X.-B.; Bu, X.-H. *Polyhedron* **2001**, *20*, 3065−3071. (b) Bu, X.-H.; Fang, Y.-Y.; Shang, Z.-L.; Zhang, R.-H.; Zhu, H.-P.; Liu, Q.-T. *Acta Crystallogr*. **1999**, *C55*, 39−40. (c) Halfen, J. A.; Fox, D. C.; Moore, H. L. To be submitted.

that biologically relevant ferrous complexes are readily prepared using L^8py_2 as a supporting ligand. Of particular significance is the isolation and structural characterization of a number of square-pyramidal Fe(II)−thiolate complexes that model the structural and magnetic properties of SOR$_{Red}$.

Experimental Section

Materials and Methods. Reagents were obtained from commercial sources and used as received unless noted otherwise. Solvents were purified according to standard methods. The tetradentate ligand L^8py_2 was prepared from 1,5-diazacyclooctane dihydrobromide as described previously.[6] Because of the hazards associated with the use of hydrazine in the published, large scale synthesis of 1,5-diazacyclooctane,[8] we present an alternative synthesis that avoids the use of this toxic material. Sodium thiolates were prepared by the reaction of the aryl- or alkylthiol with NaH in THF and isolated as white powders. All reactions were conducted and products were handled under an inert atmosphere using standard Schlenk techniques, or in a Vacuum Atmospheres inert atmosphere glovebox. NMR spectra were obtained using a JEOL Eclipse 400 spectrometer at room temperature. ^{1}H and ^{13}C{^{1}H} chemical shifts are reported versus TMS and are referenced to residual solvent peaks. Electronic absorption spectra were measured using a Hewlett-Packard 8453 spectrophotometer (190−1100 nm range). Electrochemical experiments were conducted with a BAS CV50 potentiostat, using a platinum disk working electrode, an SCE reference electrode, and a platinum wire auxiliary electrode. Cyclic voltammograms were obtained in CH$_3$CN (0.1 M n-Bu$_4$NClO$_4$) with an analyte concentration of 1 mM. Under these experimental conditions, the ferrocene/ferrocenium redox couple was observed at +461 mV (ΔE_p = 96 mV) with i_{pa}/i_{pc} = 0.92. Elemental analyses were performed by Galbraith Laboratories or by Atlantic Microlabs.

1,3-Bis(p-toluenesulfonyl)-1,3-diaminopropane. To a solution of K$_2$CO$_3$ (201.4 g, 1.456 mol) in water (0.6 L) was added 1,3-diaminopropane (54.31 g, 0.733 mol). A solution of p-toluenesulfonyl chloride (277.9 g, 1.457 mol) in THF (1.2 L) and added to the diamine solution over a period of 3 h. The heterogeneous mixture was stirred overnight and then divided into two equal portions. Each portion was poured into 1 L of ice water, causing the crude product to precipitate. The mixture was filtered and the solid washed with cold water and then dried under vacuum. Recrystallization from a minimum of hot CH$_3$CN provided the pure product as a colorless crystalline solid, 219.4 g (78%), mp 137−138 °C (lit. 138−140 °C).[9] ^{1}H NMR (400 MHz, CD$_3$CN) δ 7.67 (d, J = 8.4 Hz, 4H), 7.36 (d, J = 7.7 Hz, 4H), 5.48 (br t, J = 5.3, 2H), 2.79 (dt, J = 5.3 Hz, 4H), 2.41 (s, 6H), 1.53 (br pentet, J = 6.9 Hz, 2H) ppm; ^{13}C{^{1}H} NMR (100 MHz, acetone-d_6) δ 142.9, 138.1, 129.6, 126.9, 40.4, 29.8, 20.6 ppm.

1,3-Bis(p-toluenesulfonyloxy)propane. A solution of p-toluenesulfonyl chloride (450.6 g, 2.36 mol) in pyridine (1 L) was prepared and cooled to 3 °C. A solution of 1,3-propanediol (60.68 g, 0.797mol) in pyridine (165 mL) was added dropwise over 3 h, while maintaining the temperature of the mixture between 5 and −10 °C. The heterogeneous mixture was stored at −20 °C overnight. Slow addition of ice water (2 L) caused the crude product to precipitate. The solid was collected by filtration and washed with

(8) Mills, D. K.; Font, I.; Farmer, P. J.; Hsiao, Y.-M.; Tuntulani, T.; Buonomo, R. M.; Goodman, D. C.; Musie, G.; Grapperhaus, C. A.; Maguire, M. J.; Lai, C.-H.; Hatley, M. L.; Smee, J. J.; Bellefeuille, J. A.; Darensbourg, M. Y. *Inorg. Synth*. **1997**, *32*, 89−97.
(9) Searle, G. H.; Geue, R. J. *Aust. J. Chem*. **1984**, *37*, 959−970.

cold water (1 L). Recrystallization from a minimum of hot CH_3-CN provided the pure product as a colorless crystalline solid, 201.2 g (67%), mp 92−93 °C (lit. 91−93 °C).[9] ^{1}H NMR (400 MHz, $CDCl_3$) δ 7.73 (d, J = 8.4 Hz, 4H), 7.34 (d, J = 7.7 Hz, 4H), 4.23 (t, J = 5.9 Hz, 4H), 2.45 (s, 6H), 1.99 (pentet, J = 6.1 Hz, 2H) ppm; ^{13}C{^{1}H} NMR (100 MHz, $CDCl_3$) δ 145.4, 132.6, 130.0, 128.0, 65.9, 28.6, 21.8 ppm.

1,5-Bis(*p*-toluenesulfonyl)-1,5-diazacyclooctane. Sodium metal (7.19 g, 0.3127 mol) was dissolved in dry, degassed methanol to form a solution of sodium methoxide. To this solution was added 1,3-bis(*p*-toluenesulfonyl)-1,3-diaminopropane (59.69 g, 0.156 mol), and the resulting solution refluxed under N_2 for 2 h. After cooling, the solvent was removed under reduced pressure and the white residue thoroughly dried under vacuum. Anhydrous DMF (1 L) was added to the solid and the mixture heated to 100 °C under N_2. To this mixture was added a solution of 1,3-bis(*p*-toluenesulfonyl-oxy)propane (59.91 g, 0.156 mol) in anhydrous DMF (0.6 L) over the course of 2.5 h. The resulting amber solution was heated at 100 °C for 3 h and then cooled to room temperature. Slow addition of water (2 L) to the amber solution caused the crude product to precipitate. The solid was collected and washed successively with water (0.5 L), ethanol (0.5 L), and Et_2O (0.5 L) to provide the product as an off-white microcrystalline solid, 48.23 g (73%), mp 214−216 °C (lit. 218 °C).[10] ^{1}H NMR (400 MHz, $CDCl_3$) δ 7.67 (d, J = 8.4 Hz, 4H), 7.30 (d, J = 8.1 Hz, 4H), 3.26 (t, J = 5.9 Hz, 8H), 2.42 (s, 6H), 2.03 (pentet, J = 5.7 Hz, 4H) ppm; ^{13}C{^{1}H} NMR (100 MHz, $CDCl_3$) δ 143.4, 135.7, 129.8, 127.0, 46.9, 30.0, 21.6 ppm.

1,5-Diazacyclooctane dihydrobromide. A mixture of 1,5-bis-(*p*-toluenesulfonyl)-1,5-diazacyclooctane (47.73 g, 0.113 mol) and phenol (42.57 g, 0.452 mol) was dissolved in 33% HBr/HOAc (500 mL) under N_2 and heated to 90 °C. Care should be exercised as significant outgassing of HBr occurs while heating. After 18 h, the mixture was cooled to 60 °C, an additional portion of 33% HBr/HOAc (100 mL) was added, and the mixture was then reheated to 90 °C for 2 h. After cooling to room temperature, the precipitate was separated by filtration, washed with Et_2O (250 mL), and dried under vacuum to yield the product, 26.59 g (85%), mp > 250 °C. ^{1}H NMR (400 MHz, D_2O) δ 3.44 (t, J = 5.6 Hz, 8H), 2.30 (pentet, J = 5.7 Hz, 4H) ppm; ^{13}C{^{1}H} NMR (100 MHz, D_2O) δ 44.1, 21.1 ppm. The solid thus obtained was used for the synthesis of L^8py_2 without further purification.[6]

[$L^8py_2FeCl_2$] (1). A solution of $FeCl_2$ (0.0745 g, 0.452 mmol) in CH_3CN (2 mL) was added to a solution of L^8py_2 (0.0931 g, 0.314 mmol) in CH_3CN (2 mL), and after stirring for several minutes, a yellow-orange precipitate was deposited. The precipitate was washed with CH_3CN (2 mL) and Et_2O (5 mL) and dried under vacuum. Recrystallization from CH_2Cl_2/Et_2O provided the product as yellow-orange crystals, 0.0542 g (41%). Anal. Calcd for $C_{18}H_{24}$-Cl_2FeN_4: C, 51.09; H, 5.72; N, 13.24. Found: C, 50.81; H, 5.76; N, 13.11.

[$L^8py_2Fe(FBF_3$)]BF_4 (2). A solution of L^8py_2 (0.0921 g, 0.311 mmol) in CH_3CN (2 mL) was treated with [$Fe(H_2O)_6$]($BF_4)_2$ (0.1467 g, 0.435 mmol), generating a very light pink solution. After 30 min, Et_2O (5 mL) was added to the solution, causing the deposition of a light red oil. The supernatant was removed from the oil, and additional Et_2O (5−10 mL) was added to the clear supernatant, causing a colorless precipitate to form. Recrystallization from CH_3-CN/Et_2O provided colorless crystals of the product, 0.0695 g (43%). Anal. Calcd for $C_{18}H_{24}B_2F_8FeN_4$: C, 41.11; H, 4.60; N, 10.65. Found: C, 41.15; H, 4.70; N, 10.74.

(10) Houser, R. P.; Young, V. G., Jr.; Tolman, W. B. *J. Am. Chem. Soc.* **1996**, *118*, 2101−2102.

[$L^8py_2Fe(O_2CH$)]BF_4 (3). To a stirred solution of L^8py_2 (0.0504 g, 0.170 mmol) in CH_3OH (2 mL) was added [$Fe(H_2O)_6$]($BF_4)_2$ (0.0699 g, 0.207 mmol). This mixture was stirred until a homogeneous, light yellow solution was obtained. Sodium formate (0.0178 g, 0.261 mmol) was then added, and a pale yellow color was generated. After 30 min, the solvent was removed under vacuum, producing a pale yellow solid. This solid was extracted into CH_2Cl_2, the mixture filtered through Celite, and the filtrate evaporated under vacuum. The solid thus produced was recrystallized from CH_2Cl_2/Et_2O to provide pale yellow crystals of the product, 0.0361 g (44%). Anal. Calcd for $C_{19}H_{25}BF_4FeN_4O_2$: C, 47.14; H, 5.21; N, 11.57. Found: C, 47.35; H, 5.12; N, 11.55.

[$L^8py_2Fe(O_2CCH_3$)]BF_4 (4). To a stirred solution of L^8py_2 (0.0651 g, 0.220 mmol) in CH_3CN (3 mL) was added [$Fe(H_2O)_6$]-($BF_4)_2$ (0.0762 g, 0.226 mmol) followed by sodium acetate (0.0240 g, 0.292 mmol). The color of the mixture slowly changed from light pink to yellow. After stirring overnight, the solvent was removed under vacuum, and the resulting solid was extracted into CH_2Cl_2. The mixture was then filtered and the filtrate evaporated to dryness. Recrystallization of the crude yellow solid from CH_3-CN/Et_2O provided yellow crystals of the product, 0.0670 g (61%). Anal. Calcd for $C_{20}H_{27}BF_4FeN_4O_2$: C, 48.22; H, 5.46; N, 11.25. Found: C, 48.91; H, 5.75; N, 11.57.

[$L^8py_2Fe(SC_6H_4$-*p*-CH_3)]BF_4 (5). To a stirred solution of L^8-py_2 (0.0510 g, 0.172 mmol) in CH_3OH (2 mL) was added [Fe-($H_2O)_6$]($BF_4)_2$ (0.0592 g, 0.175 mmol). This mixture was stirred until a homogeneous, light yellow solution was obtained. Sodium 4-methylbenzenethiolate (0.0402 g, 0.275 mmol) was then added, and a dark yellow color was immediately generated, followed rapidly by the deposition of a yellow microcrystalline precipitate. The mixture was filtered and the solid recrystallized from CH_2-Cl_2/Et_2O to provide yellow crystals of the product, 0.0747 g (77%). Anal. Calcd for $C_{25}H_{31}BF_4FeN_4S$: C, 53.04; H, 5.58; N, 9.96. Found: C, 52.34; H, 5.49; N, 9.91.

[$L^8py_2Fe(SC_6H_4$-*m*-CH_3)]BF_4 (6). To a stirred solution of L^8-py_2 (0.0497 g, 0.168 mmol) in CH_3OH (2 mL) was added [Fe-($H_2O)_6$]($BF_4)_2$ (0.0628 g, 0.186 mmol). This mixture was stirred until a homogeneous, light yellow solution was obtained. Sodium 3-methylbenzenethiolate (0.0395 g, 0.271 mmol) was then added, and a dark yellow color was immediately generated, followed rapidly by the deposition of a yellow microcrystalline precipitate. The mixture was filtered, and the solid recrystallized from CH_2-Cl_2/Et_2O to provide yellow crystals of the product, 0.0651 g (69%). Anal. Calcd for $C_{25}H_{31}BF_4FeN_4S$: C, 53.04; H, 5.58; N, 9.96. Found: C, 52.34; H, 5.74; N, 10.05.

[$L^8py_2Fe(SC_6H_{11}$)]BF_4 (7). To a stirred solution of L^8py_2 (0.0654 g, 0.221 mmol) in CH_3OH (4 mL) was added [$Fe(H_2O)_6$]($BF_4)_2$ (0.0775 g, 0.230 mmol) followed by sodium cyclohexanethiolate (0.0450 g, 0.326 mmol). The color of the solution changed quickly to yellow, and a small amount of a yellow solid was deposited. After stirring 30 min, the volume of the mixture was reduced under vacuum, causing additional yellow solid to be deposited. The light yellow supernatant was decanted from the solid, which was dried and then redissolved in CH_2Cl_2. This yellow solution was filtered through a plug of glass wool; vapor diffusion of Et_2O into the yellow filtrate provided the product as yellow crystals, 0.0573 g (47%). Anal. Calcd for $C_{24}H_{35}BF_4FeN_4S$: C, 52.00; H, 6.36; N, 10.11. Found: C, 50.92; H, 6.19; N, 10.29.

X-ray Crystallography. Single crystals were mounted in thin-walled glass capillaries and transferred to an Enraf-Nonius CAD4 X-ray diffractometer for data collections at 25 °C using graphite monochromated Mo Kα (λ = 0.71073 Å) radiation. Unit cell constants were determined from a least squares refinement of the

Table 1. Summary of X-ray Crystallographic Data for Complexes **1**−**4**[a]

	1	2	3	4
empirical formula	$C_{18}H_{24}Cl_2FeN_4$	$C_{18}H_{24}B_2F_8FeN_4$	$C_{19}H_{25}BF_4FeN_4O_2$	$C_{20}H_{27}BF_4FeN_4O_2$
fw	423.16	525.88	484.09	498.12
cryst syst	monoclinic	orthorhombic	monoclinic	monoclinic
space group	$C2/c$	$Pnnm$	$P2_1/c$	$P2_1/n$
a (Å)	22.786(6)	16.948(1)	11.889(2)	16.325(4)
b (Å)	7.8401(5)	11.274(2)	13.666(2)	8.093(1)
c (Å)	13.805(4)	12.141(1)	14.078(2)	17.075(5)
α (deg)	90	90	90	90
β (deg)	126.94(2)	90	109.22(2)	96.72(3)
γ (deg)	90	90	90	90
V (Å^3)	1971.1(8)	2319.8(5)	2159.8(6)	2240.4(9)
Z	4	4	4	4
d_{calcd} (Mg·m^{-3})	1.426	1.506	1.489	1.477
cryst size (mm^3)	$0.40 \times 0.35 \times 0.15$	$0.48 \times 0.30 \times 0.12$	$0.35 \times 0.32 \times 0.30$	$0.42 \times 0.30 \times 0.08$
abs coeff (mm^{-1})	1.044	0.727	0.756	0.731
2 Θ max (deg)	49.96	49.96	52.06	52.08
transmission range	1.0−0.9154	1.0−0.9240	1.0−0.9225	1.0−0.8829
no. reflns collected	1779	2144	4457	4564
no. indep reflns	1734	2144	4248	4407
no. obsd reflns	1339	1489	2721	2931
no. variables	141	187	336	289
R1 (wR2)[b] [$I > 2\sigma(I)$]	0.0313 (0.0726)	0.0543 (0.1442)	0.0633 (0.1260)	0.0686 (0.1408)
GOF (F^2)	1.039	1.030	1.010	1.031
diff peaks (e$^-$·Å^{-3})	0.216, −0.240	0.550, −0.478	0.303, −0.282	0.596, −0.393

[a] See Experimental Section for additional data collection, reduction, and structure solution and refinement details. [b] R1 = $\sum||F_o| - |F_c||/\sum|F_o|$; wR2 = $[\sum[w(F_o^2 - F_c^2)^2]]^{1/2}$ where $w = 1/\sigma^2(F_o^2) + (aP)^2 + bP$.

setting angles of 25 intense, high angle reflections. Intensity data were collected using the $\omega/2\theta$ scan technique to a maximum 2θ value of 50−52°. Absorption corrections were applied based on azimuthal scans of several reflections for each sample. The data were corrected for Lorentz and polarization effects and converted to structure factors using the teXsan for Windows crystallographic software package.[11] Space groups were determined based on systematic absences and intensity statistics. Successful direct-methods solutions were calculated for each compound using the SHELXTL suite of programs.[12] Any non-hydrogen atoms not identified from the initial E-map were located after several cycles of structure expansion and full matrix least squares refinement on F^2. Hydrogen atoms were added geometrically. All non-hydrogen atoms were refined with anisotropic displacement parameters, while hydrogen atoms were refined using a riding model with group isotropic displacement parameters. Relevant crystallographic information for the compounds is summarized in Tables 1 and 2, and selected bond interatomic distances and angles are provided in Tables 3 and 4. Complete crystallographic data for each compound are provided as Supporting Information in CIF format.

Neutral molecules of **1** reside on a crystallographic 2-fold axis. The propylene chains of the diazacyclooctane backbone are disordered over two equally occupied orientations. A crystallographic mirror plane bisects both the cation and the uncoordinated BF$_4^-$ counterion in **2**. This ion is rotationally disordered over two equally occupied orientations. Geometric constraints were applied to the uncoordinated anion, and the anisotropic displacement parameters for the atoms of this ion were restrained to fit a rigid bond approximation. The formate ligand in **3** is disordered over

(11) *TeXsan for Windows*, V 1.02; Molecular Structure Corporation, Inc.: The Woodlands, TX.
(12) *SHELXTL*, V. 5.1 for Windows NT; Bruker AXS: Madison, WI.

Table 2. Summary of X-ray Crystallographic Data for Iron(II)−Thiolate Complexes **5**−**7**[a]

	5	6	7
empirical formula	$C_{25}H_{31}BF_4FeN_4S$	$C_{25}H_{31}BF_4FeN_4S$	$C_{24}H_{35}BF_4FeN_4S$
fw	562.26	562.26	554.28
cryst syst	triclinic	triclinic	monoclinic
space group	$P\bar{1}$	$P\bar{1}$	$C2/m$
a (Å)	10.396(2)	10.791(1)	17.532(3)
b (Å)	11.091(2)	10.971(2)	12.157(1)
c (Å)	13.142(6)	13.262(2)	14.028(3)
α (deg)	89.93(3)	91.74(1)	90
β (deg)	111.04(3)	110.55(1)	112.18(2)
γ (deg)	114.00(3)	115.04(1)	90
V (Å^3)	1339.4(7)	1302.0(3)	2768.6(8)
Z	2	2	4
d_{calcd} (Mg·m^{-3})	1.394	1.434	1.330
cryst size (mm^3)	$0.52 \times 0.32 \times 0.10$	$0.50 \times 0.45 \times 0.40$	$0.52 \times 0.38 \times 0.36$
abs coeff (mm^{-1})	0.690	0.710	0.666
2 Θ max (deg)	50.14	50.04	49.98
transmission range	1.0−0.8984	1.0−0.9386	1.0−0.9160
no. reflns collected	4911	4855	2651
no. indep reflns	4643	4590	2560
no. obsd reflns	2591	4020	1782
no. variables	325	325	193
R1 (wR2)[b] [$I > 2\sigma(I)$]	0.0755 (0.1702)	0.0396 (0.0947)	0.0599 (0.1443)
GOF (F^2)	1.014	1.032	1.024
diff peaks (e$^-$·Å^{-3})	0.630, −0.393	0.552, −0.384	0.330, −0.267

[a] See Experimental Section for additional data collection, reduction, and structure solution and refinement details. [b] R1 = $\sum||F_o| - |F_c||/\sum|F_o|$; wR2 = $[\sum[w(F_o^2 - F_c^2)^2]]^{1/2}$ where $w = 1/\sigma^2(F_o^2) + (aP)^2 + bP$.

two equivalent positions with occupancies 77(1)% and 23(1)%, and the BF$_4^-$ counterion is rotationally disordered over two positions with occupancies 71(1)% and 29(1)%. The refinements of **4**−**6** proceeded without complication. A crystallographic mirror plane bisects the cation in **7**. The carbon atoms of the cyclohexyl group exhibit high anisotropic displacement parameters, reflecting the room-temperature data collection for this complex. The BF$_4^-$ anion in **7** is also disordered over two equally occupied orientations; geometric constraints were applied to the atoms of this ion.

Results and Discussion

Synthesis. The primary reactions conducted as part of this study are illustrated in Scheme 1. Among the complexes initially targeted for synthesis were those that contain an iron-(II) ion bound by both the tetradentate ligand L^{8}py$_2$ as well as by some other, labile group(s) that could be readily replaced by a more biologically relevant thiolate coligand. The first such complex, [L^{8}py$_2$FeCl$_2$] (**1**), was isolated as yellow-orange crystals upon combination of L^{8}py$_2$ with anhydrous FeCl$_2$ in CH$_3$CN. While **1** does contain labile chloride ligands, it proved to be an ineffective precursor for further synthetic studies, as demonstrated by its reaction with sodium formate. This reaction did not result in simple substitution of a chloride ligand by a formate ion; rather, the sole iron-containing product of this reaction was [L^{8}py$_2$FeCl]$_2$[Fe$_2$Cl$_6$], isolated as light yellow crystals and identified by X-ray crystallography.[13] The isolation of this product, co-deposited with colorless crystals of the free ligand L^{8}py$_2$,[14] indicates that conversion of **1** to its monochloride-ligated derivative is thermodynamically favored over substitution of the precursor's chloride ligand(s).

A more viable synthetic precursor was identified in [L^{8}py$_2$Fe(FBF$_3$)]BF$_4$ (**2**), isolated as colorless crystals from the

Table 3. Significant Interatomic Distances (Å) and Angles (deg) for Complexes **1**–**4**

	1			**2**	
Fe−N1	2.334(2)		Fe−N1	2.205(4)	
Fe−N2	2.305(2)		Fe−N2	2.166(4)	
Fe−Cl1	2.4283(8)		Fe−F1	1.967(4)	
N1−Fe−N1A	76.4(1)		B1−F1	1.39(1)	
N1−Fe−N2	71.40(8)		B1−F2	1.341(8)	
N1−Fe−N2A	130.88(8)		B1−F3	1.353(8)	
N1−Fe−Cl1	91.75(6)		B1−F4	1.35(1)	
N1−Fe−Cl1A	133.78(6)		N1−Fe−N1A	88.5(2)	
N2−Fe−N2A	155.3(1)		N1−Fe−N2	77.6(1)	
N2−Fe−Cl1	83.82(6)		N1−Fe−N2A	145.6(1)	
N2−Fe−Cl1A	84.91(6)		N1−Fe−F1	114.6(1)	
Cl1−Fe−Cl1A	125.25(5)		N2−Fe−N2A	107.2(2)	
			N2−Fe−F1	98.6(1)	
			Fe−F1−B1	133.1(4)	

	3			**4**	
Fe−N1	2.214(4)		Fe−N1	2.202(4)	
Fe−N2	2.195(3)		Fe−N2	2.195(4)	
Fe−N3	2.140(4)		Fe−N3	2.159(4)	
Fe−N4	2.198(4)		Fe−N4	2.215(4)	
Fe−O1	1.987(5)		Fe−O1	2.009(4)	
Fe···O2	2.85(1)		Fe···O2	2.565(4)	
C19−O1	1.223(8)		C19−O1	1.265(6)	
C19−O2	1.209(8)		C19−O2	1.240(6)	
N1−Fe−N2	81.2(1)		N1−Fe−N2	81.0(2)	
N1−Fe−N3	77.2(2)		N1−Fe−N3	78.2(1)	
N1−Fe−N4	140.6(1)		N1−Fe−N4	133.1(1)	
N1−Fe−O1	129.0(2)		N1−Fe−O1	133.6(2)	
N2−Fe−N3	146.3(1)		N2−Fe−N3	148.6(2)	
N2−Fe−N4	76.1(1)		N2−Fe−N4	74.6(2)	
N2−Fe−O1	101.5(2)		N2−Fe−O1	96.5(2)	
N3−Fe−N4	105.3(2)		N3−Fe−N4	103.5(2)	
N3−Fe−O1	112.3(2)		N3−Fe−O1	114.9(2)	
N4−Fe−O1	87.3(2)		N4−Fe−O1	89.0(2)	
O2···Fe−O1	48.5(2)		O2···Fe−O1	55.1(1)	
O2···Fe−N1	82.7(2)		O2···Fe−N1	84.0(1)	
O2···Fe−N2	111.7(2)		O2···Fe−N2	115.3(1)	
O2···Fe−N3	91.0(2)		O2···Fe−N3	85.7(1)	
O2···Fe−N4	135.7(2)		O2···Fe−N4	142.7(1)	
O1−C19−O2	122.7(7)		O1−C19−O2	120.2(5)	

Table 4. Significant Interatomic Distances (Å) and Angles (deg) for Iron(II)−Thiolate Complexes **5**−**7**

	5			**6**	
Fe−N1	2.241(5)		Fe−N1	2.225(2)	
Fe−N2	2.212(6)		Fe−N2	2.217(2)	
Fe−N3	2.185(5)		Fe−N3	2.182(2)	
Fe−N4	2.197(5)		Fe−N4	2.171(2)	
Fe−S1	2.323(3)		Fe−S1	2.3060(9)	
N1−Fe−N2	80.6(2)		N1−Fe−N2	80.01(8)	
N1−Fe−N3	75.3(2)		N1−Fe−N3	75.54(8)	
N1−Fe−N4	147.3(2)		N1−Fe−N4	147.24(8)	
N1−Fe−S1	104.1(2)		N1−Fe−S1	105.36(6)	
N2−Fe−N3	136.8(2)		N2−Fe−N3	136.00(8)	
N2−Fe−N4	77.0(2)		N2−Fe−N4	77.80(8)	
N2−Fe−S1	111.2(2)		N2−Fe−S1	112.05(6)	
N3−Fe−N4	105.8(2)		N3−Fe−N4	104.92(8)	
N3−Fe−S1	109.2(2)		N3−Fe−S1	109.44(6)	
N4−Fe−S1	106.1(2)		N4−Fe−S1	107.17(6)	
Fe−S1−C19	97.6(2)		Fe−S1−C19	95.25(9)	

	7	
Fe−N1	2.228(4)	
Fe−N2	2.189(4)	
Fe−S1	2.259(2)	
N1−Fe−N1A	79.4(2)	
N1−Fe−N2	76.1(2)	
N1−Fe−N2A	140.8(1)	
N1−Fe−S1	108.9(1)	
N2−Fe−N2A	105.3(2)	
N2−Fe−S1	107.8(1)	
Fe−S1−C11	100.9(4)	

Most significant is the ability of **2** to be transformed into structural models of SOR_{Red} via its reaction with aromatic or aliphatic thiolates. For example, reaction of **2** with the sodium salts of *para*- or *meta*-methylbenzenethiolate provided yellow-orange crystals of $[L^8py_2Fe(SC_6H_4$-*p*-$CH_3)]BF_4$ (**5**) and $[L^8py_2Fe(SC_6H_4$-*m*-$CH_3)]BF_4$ (**6**), respectively. These compounds were conveniently isolated in pure form by filtration from the crude reaction mixture. In a similar manner, reaction of **2** with sodium cyclohexanethiolate produced yellow crystals of $[L^8py_2Fe(SC_6H_{11})]BF_4$ (**7**). The alkylthiolate ligation of this complex closely models the cysteine thiolate ligand present in SOR_{Red}. Crystallographic analyses confirm that these thiolate-ligated iron(II) complexes replicate the structure of the SOR_{Red} active site.

Structural Characterization. X-ray crystallographic data for the complexes are collected in Tables 1 and 2, while significant interatomic distances and angles are compiled in Tables 3 and 4. Full listings of positional and anisotropic displacement parameters, as well as complete tables of interatomic distances and angles in CIF format, are provided as Supporting Information.

The X-ray crystal structure of **1** reveals a hexacoordinate iron(II) ion bound by tetradentate L^8py_2 as well as by two chloride ions (Figure 2). The iron(II) center adopts an uncommon trigonal prismatic geometry, presumably because of unfavorable steric interactions that would occur between the two chloride ligands and the propylene chains of the macrocyclic backbone if the complex were to adopt a more regular, octahedral geometry. Indeed, the six-membered chelate rings in **1** both adopt chair conformations, presumably to minimize these steric interactions. The metal−ligand bond
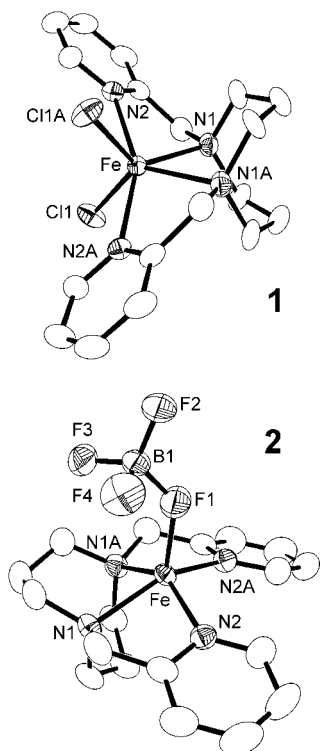
reaction of L^8py_2 with $[Fe(H_2O)_6](BF_4)_2$ in CH_3CN. This compound is noteworthy not only because it contains a labile η^1-BF_4^- ligand but also because this tetrafluoroborate ligand is able to compete so effectively with other, more strongly donating H_2O and CH_3CN ligands for a vacant (axial) coordination position on the iron center. Facile substitution of the tetrafluoroborate ligand was demonstrated by the reaction of **2** with carboxylate ions. Mixing **2** with sodium formate in CH_3OH produced pale yellow crystals of $[L^8py_2Fe(O_2CH)]BF_4$ (**3**), while a parallel reaction with sodium acetate generated yellow crystals of $[L^8py_2Fe(O_2CCH_3)]BF_4$ (**4**).

(13) X-ray crystallographic data for $[L^8py_2FeCl]_2[Fe_2Cl_6]$, $C_{36}H_{46}Cl_8$-Fe_4N_8: triclinic, $P\bar{1}$, with $a = 8.358(2)$ Å, $b = 10.968(2)$ Å, $c = 12.938(3)$ Å, $\alpha = 77.29(3)°$, $\beta = 85.48(3)°$, $\gamma = 77.41(3)°$, $V = 1128.6(4)$ Å^3, and $Z = 1$ at 25 °C. Full matrix least squares refinement on F^2 provided current residuals $R1 = 0.0530$, $wR2 = 0.1481$, and GOF = 1.031 for 1641 reflections with $I > 2\sigma(I)$ and 163 variables. Full details of the structure determination will be reported elsewhere.

(14) X-ray crystallographic data for L^8py_2, $C_{18}H_{22}N_4$: triclinic, $P\bar{1}$, with $a = 6.259(1)$ Å, $b = 11.198(3)$ Å, $c = 13.047(3)$ Å, $\alpha = 113.28(2)°$, $\beta = 94.18(2)°$, $\gamma = 90.02(2)°$, $V = 837.3(3)$ Å^3, and $Z = 2$ at 25 °C. Full matrix least squares refinement on F^2 provided current residuals $R1 = 0.0587$, $wR2 = 0.1516$, and GOF = 1.015 for 1604 reflections with $I > 2\sigma(I)$ and 199 variable parameters. Full details of the structure determination will be reported elsewhere.

Figure 2. Thermal ellipsoid representations (35% probability level), with partial atom labeling schemes, of **1** and **2**. Hydrogen atoms and uncoordinated BF_4^- ions are omitted for clarity.

Figure 3. Thermal ellipsoid representations (35% probability level), with partial atom labeling schemes, of the cationic portions of **3** and **4**. Hydrogen atoms are omitted for clarity.

lengths in **1** are uniformly longer than those identified for the remainder of the complexes reported herein, reflecting the high coordination number of the iron center in this complex. These structural features contrast with those of the cation present in **2** (Figure 2) in which the tetradentate L^8-py$_2$ ligand occupies four equatorial coordination sites of the square-pyramidal iron(II) complex, complemented by an η^1-BF_4^- ligand bound in one axial position. Inspection of the six-membered chelate rings in **2** reveals that one of them (opposite the BF_4^- ligand) adopts a boat conformation; similar coordination-number-dependent chelate ring conformations in tetradentate ligands derived from diazacyclooctane have been discussed previously.[15] The iron(II) ion in **2** resides 0.59 Å above the plane of the four basal nitrogen donors, displaced toward the axial BF_4^- group. The Fe–F bond length, 1.967(4) Å, is shorter than that present in the only other iron–tetrafluoroborate complex structurally characterized to date, [Fe(η^1-BF_4)(CO)(depe)$_2$]BF_4 (Fe–F = 2.081-(6) Å), presumably because **2** lacks an additional donor group *trans* to its BF_4^- ligand.[16] As expected, the terminal B–F bonds are shorter than that present in the B–F–Fe unit. Complex **2** has proven to be a versatile starting material for the synthesis of numerous pentacoordinate iron(II) complexes of L^8py$_2$.

The X-ray crystal structures of formate complex **3** and acetate complex **4** reveal iron(II) complexes with distorted pentacoordinate geometries, in which the Fe–O(1) bonds
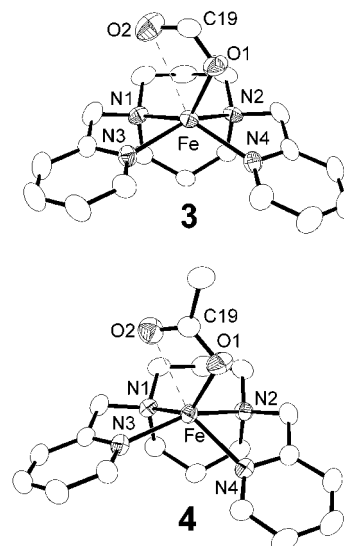
are significantly displaced from the position normally occupied by a metal–axial ligand bond in a square-pyramidal transition metal complex (Figure 3). These deviations from ideal geometry are most apparent in the O(1)–Fe–N(1) bond angles, 129.0(2)° in **3** and 133.6(2)° in **4**, which are significantly perturbed from the ideal value of 90°. The distorted geometries adopted by these complexes presumably reflect weak binding of the second carboxylate oxygen atoms to the iron centers. Weak interactions between the iron centers and the dangling carboxylate oxygen atoms are indicated by the Fe–O(2) distances (2.85(1) Å in **3** and 2.565(4) Å in **4**), the small amount of C–O bond length alternation in the carboxylate ions (Δ_{C-O} = 0.014(8) Å for **3** and 0.025(6) Å for **4**), and also the lengths of the Fe–N(4) bonds, which are approximately *trans* to the Fe···O(2) interactions. In both complexes, the Fe–N(4) bonds are elongated relative to the Fe–N(3) bonds (by 0.058(4) Å in **3** and 0.056(4) Å in **4**), a bond length asymmetry that is absent in the remainder of the pentacoordinate complexes described herein. The asymmetric bidentate coordination of the carboxylate ions in **3** and **4**, in conjunction with the ligation of the poor donor BF_4^- in their common precursor **2**, may reflect significant Lewis acidity of the iron(II) center in complexes of L^8py$_2$.

The ultimate targets of the current synthetic study were pentacoordinate iron(II)–thiolate complexes, and three such compounds, **5**–**7**, were isolated in forms amenable to crystallographic analysis (Figure 4). These iron(II)–thiolate complexes share a common structural motif: all contain a regular, square-pyramidal iron(II) center, with a basal plane of four nitrogen donors provided by the tetradentate L^8py$_2$ ligand, complemented by an axial aryl- or alkylthiolate donor. As was the case in the other square-pyramidal iron(II) complexes described previously, the iron(II) ions in the thiolate complexes are displaced from the basal plane of four nitrogen donors toward the axial thiolate ligands (by 0.67, 0.67, and 0.69 Å, in **5**, **6**, and **7**, respectively). The Fe–S bond lengths in the iron(II)–thiolate complexes are some-

(15) Buonomo, R. M.; Reibenspies, J. J.; Darensbourg, M. Y. *Chem. Ber.* **1996**, *129*, 779–784.
(16) depe = 1,2-bis(diethylphosphino)ethane: Landau, S. E.; Morris, R. H.; Lough, A. J. *Inorg. Chem.* **1999**, *38*, 6060–6068.
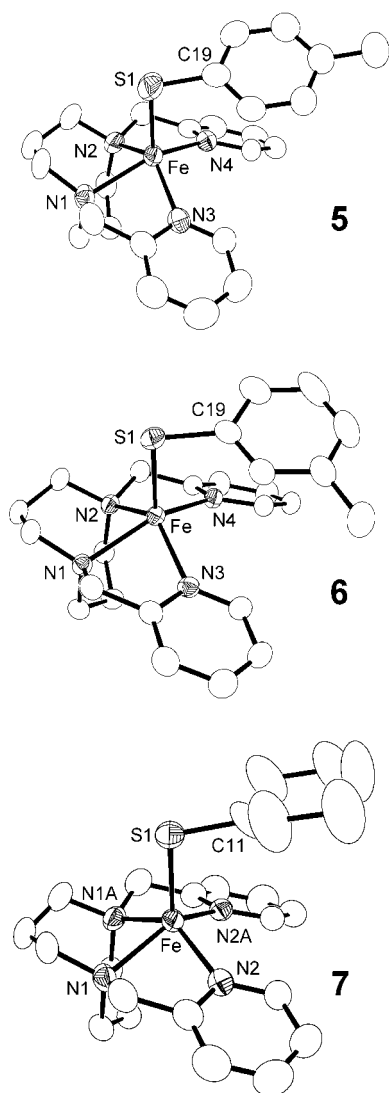
5

6

7

Figure 4. Thermal ellipsoid representations (35% probability level), with partial atom labeling schemes, of the cationic portions of **5**−**7**. Hydrogen atoms are omitted for clarity.

what sensitive to the nature of the thiolate ligands, spanning a range of 2.259(2)−2.323(3) Å in the three complexes described herein. The Fe−S bond length in **7** is the shortest in this series, perhaps reflecting the increased electron-donating ability of the aliphatic thiolate relative to the aromatic thiolates. With their square-pyramidal geometries, basal planes of four neutral nitrogen donors, and vacant coordination sites *trans* to their axial thiolate ligands, iron-(II)−thiolate complexes **5**−**7** model the $[Fe^{II}(N_{his})_4(S_{cys})]$ structure of SOR_{Red}.[4] Specific comparisons between the metrical parameters of SOR_{Red} and its synthetic models are provided in Figure 5.

The compounds with structures most closely related to **5**−**7** are square-pyramidal iron(II)−thiolate complexes, including several porphyrin-supported iron(II)−thiolate species,[17] as well as the Schiff-base-ligated complex $Et_4N[(5-NO_2salen)Fe(SC_6H_4\text{-}p\text{-}CH_3)]$.[18] The porphyrin-ligated compounds model the high-spin ferrous state of the heme enzyme cytochrome P-450,[19] and as a result, detailed comparisons between these complexes and **5**−**7** are tenuous because of

the structural and electronic differences between the porphyrin ligands and L^8py_2. The structure of the Schiff base complex is quite similar to those of **5**−**7**, although the N_2O_2 basal donor set provided by the 5-NO_2salen^{2-} ligand fails to replicate the array of biological donor groups present in the SOR active site. Also relevant to the iron(II)−thiolate complexes reported herein are two non-heme iron(II) complexes with N_4S donor sets, $[(TPA)Fe(SC_6H_2\text{-}2,4,6\text{-}(CH_3)_3)]$-$ClO_4$[20] and $[FeS^{Me2}N_4(tren)]PF_6$, the latter of which is oxidized to a stable Fe(III) analogue by O_2^-.[21] While the trigonal-bipyramidal geometries of these two complexes do not replicate the square-pyramidal structure of SOR_{Red}, the latter compound does model SOR reactivity.

Physical, Spectroscopic, and Electrochemical Properties of SOR Model Complexes. The metal−ligand bond lengths identified by X-ray crystallography suggest that the iron-(II)−thiolate complexes contain high-spin ($S = 2$) iron(II) ions.[22] These assignments were confirmed by solid-state magnetic susceptibility measurements (Table 5), which provided magnetic susceptibilities ranging from 4.52 to 5.27 μ_B for the complexes described previously. Of particular significance is that the $S = 2$ ground state of these iron-(II)−thiolate complexes replicates that of SOR_{Red}.[3b,4c] With the exception of tetrafluoroborate-ligated complex **2**, the iron-(II) complexes of L^8py_2 are yellow in color, the result of electronic transitions in the high-energy region of the visible spectrum (Table 5). The electronic absorption spectra of the iron(II)−thiolate complexes are complex, because of multiple overlapping transitions between 300 and 425 nm; such complexity is not apparent in the optical spectra of complexes **2**−**4**, which lack axial thiolate ligation. For example, the UV−vis spectrum of **7** (Figure 6), whose axial cyclohex-anethiolate ligand best models the cysteinate donor present in SOR_{Red}, was fit by four overlapping Gaussian transitions centered at 254 nm (7000 M^{-1} cm^{-1}), 305 nm (830 M^{-1} cm^{-1}), 340 nm (1800 M^{-1} cm^{-1}), and 424 nm (300 M^{-1} cm^{-1}). While a detailed analysis of these visible spectroscopic features is not supported by the available data, it seems reasonable to suggest that one or more of these transitions may result from a thiolate-to-iron(II) LMCT transition, as recently identified for SOR_{Red}; in the enzyme from *Pyrococcus furiosus*, charge-transfer transitions involving the iron-

(17) (a) Schappacher, M.; Ricard, L.; Weiss, R.; Montiel-Montoya, R.; Gonser, E.; Bill, E.; Trautwein, A. X. *Inorg. Chim. Acta* **1983**, *78*, L9−L12. (b) Schappacher, M.; Ricard, L.; Fischer, J.; Weiss, R.; Montiel-Montoya, R.; Bill, E.; Trautwein, A. X. *Inorg. Chem.* **1989**, *28*, 4639−4645. (c) Caron, C.; Mitschler, A.; Riviere, G.; Ricard, L.; Schappacher, M.; Weiss, R. *J. Am. Chem. Soc.* **1979**, *101*, 7401−7402.

(18) 5-NO$_2$salen = 1,2-bis-(5-nitrosailcylidineamino)ethane: Mukherjee, R. N.; Abrahamson, A. J.; Patterson, G. S.; Stack, T. D. P.; Holm, R. H. *Inorg. Chem.* **1988**, *27*, 2137−2144.

(19) Sono, M.; Roach, M. P.; Coulter, E. D.; Dawson, J. H. *Chem. Rev.* **1996**, *96*, 2841−2887.

(20) TPA = tris(2-pyridylmethyl)amine: Zang, Y.; Que, L., Jr. *Inorg. Chem.* **1995**, *34*, 1030−1035.

(21) S^{Me2}N$_4$(tren) = 3-{2-[bis(2-aminoethyl)amino]ethylimino}-2-methylbutane-2-thiol: Shearer, J.; Nehring, J.; Lovell, S.; Kaminsky, W.; Kovacs, J. A. *Inorg. Chem.* **2001**, *40*, 5483−5484.

(22) (a) Blakesley, D. W.; Payne, S. C.; Hagen, K. S. *Inorg. Chem.* **2000**, *39*, 1979−1989. (b) Diebold, A.; Hagen, K. S. *Inorg. Chem.* **1998**, *37*, 215−223.
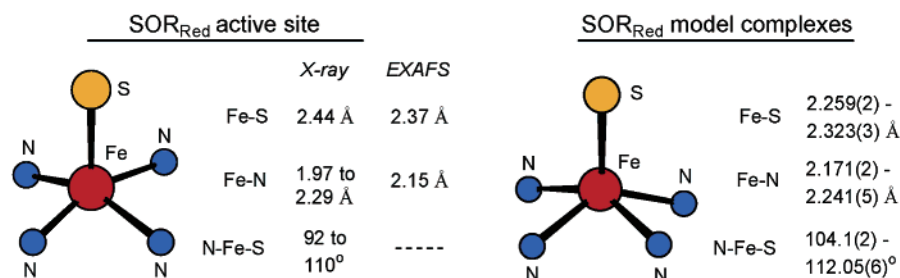
Figure 5. Core structures of SOR$_{Red}$ and its synthetic models **5**−**7**, with significant metrical details noted. Bond lengths and angles for SOR$_{Red}$ are taken from refs 4b (single-crystal X-ray, high-occupancy iron site "A") and 4c (EXAFS).

Table 5. Magnetic Susceptibility, UV−Vis Spectroscopic, and Electrochemical Data

complex	μ_{eff} (μ_B)[a]	λ_{max}, nm (ϵ, M^{-1} cm^{-1})[b]	E_{pa} (mV)[c]
2	4.85	261 (9600), sh 332 (790)	+1228
3	4.92	262 (8000), 364 (420)	+941
4	4.52	261 (6400), 374 (440)	+844
5	5.27	255 (14000), sh 309 (3400), sh 405 (820)	+615
6	4.98	269 (13000), sh 305 (3100), sh 402 (570)	+655
7	4.70	254 (7000), sh 305 (830), 340 (1800), sh 424 (300)	+565

[a] Solid-state magnetic susceptibility determined at room temperature. [b] Measured in CH$_3$CN (sh = shoulder). [c] Measured in CH$_3$CN with 0.1 M Bu$_4$NClO$_4$. Potentials are quoted versus SCE at a scan rate of 100 mV·sec^{-1}.
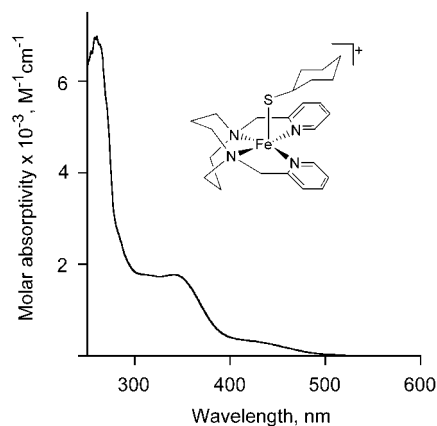

Figure 6. Electronic absorption spectrum of **7** in CH$_3$CN.

(II) center occur at 295 nm (identified by MCD) and 320 nm.[4c] Examination of **5**−**7** by MCD and resonance Raman spectroscopy may clarify the nature of the optical transitions observed in these iron(II)−thiolate complexes.

The redox chemistry of iron(II)−thiolate complexes **5**−**7** was probed using electrochemical methods. At room temperature, **5**−**7** exhibit irreversible oxidation processes in their cyclic voltammograms (Table 5), with anodic peak potentials (E_{pa}) that are uniformly higher than that of the reversible Fe(II)/Fe(III) redox potential of SOR ($E°$ = −33(4) mV versus SCE for the SOR from *Treponema pallidum*, −2(10) mV versus SCE for the SOR from *P. furiosus*).[3b,4c] The divergence among the redox potentials of **5**−**7** and those of SOR is at least partially rooted in the different solvent systems used for the electrochemical measurements (CH$_3$-CN for **5**−**7**; aqueous, pH = 7.5−7.8 buffer for SOR).[3b,4c] Unfortunately, the low solubility of **5**−**7** in water precludes determination of their redox potentials in aqueous solution.

The oxidation potentials of iron(II)−thiolate complexes **5**−**7** are uniformly lower than those of **2**, **3**, or **4**, reflecting increased electron densities at the iron(II) centers in the thiolate complexes relative to those in the tetrafluoroborate and carboxylate complexes. Moreover, the anodic peak potentials of the thiolate complexes reflect the relative electron-donating abilities of the bound thiolate ligands. Thus, the oxidation potential of **7**, which contains the most electron rich, aliphatic thiolate ligand, is lower than those of **5** and **6**, which contain less electron rich, aromatic thiolate ligands. The irreversibility of all of these oxidative processes suggests that the electrochemically generated iron(III)−thiolate complexes undergo decomposition in solution, preventing their facile electrochemical reduction to the original iron(II)−thiolate state. We speculate that this reaction is a bimolecular process in which two iron(III)−thiolate complexes undergo an internal redox reaction to form 2 equiv of an unidentified iron(II) complex and 1 equiv of a disulfide. In support of this notion, chemical oxidation of **5** with AgPF$_6$ in CH$_2$Cl$_2$ produced *p*-tolyl disulfide, identified by GC/MS analysis of the resultant solution; similar reactivity was observed previously for the Schiff base-ligated iron(II)−thiolate complex Et$_4$N[(5-NO$_2$salen)Fe(SC$_6$H$_4$-*p*-CH$_3$)].[18] Finally, while **5**−**7** are irreversibly oxidized at room temperature, the cyclic voltammogram of **7** at −20 °C reveals an electrochemically reversible (ΔE_p = 87 mV) but chemically quasireversible (i_{pc}/i_{pa} = 0.6) redox couple with $E°'$ = 470 mV versus SCE. Thus, chemical oxidation of **7** to its (metastable) Fe(III)−thiolate redox partner may be possible under conditions of reduced temperatures and/or high dilution. Efforts to generate and characterize such a species are ongoing.

Summary

We have prepared and characterized a family of iron(II)−thiolate complexes that model the square-pyramidal [Fe^{II}-(N$_{his}$)$_4$(S$_{cys}$)] structure and high-spin, S = 2 electronic ground state of the reduced active site of superoxide reductase. Electrochemical studies at ambient temperature reveal that the oxidized forms of these complexes are unstable relative to the formation of organic disulfides and thus indicate that further tuning of the structural and/or electronic properties of this family of model compounds is necessary to replicate the facile one-electron redox cycling that is characteristic of the enzyme. Ongoing synthetic, spectroscopic, and reactivity studies of compounds that model SOR$_{Red}$ may provide

significant insights into superoxide detoxification pathways in biological systems.

Supporting Information Available: Complete X-ray crystallographic information in CIF format. This material is available free of charge on the Internet at http://pubs.acs.org.

IC025517L